Inorganic Chemistry

Article

pubs.acs.org/IC

Iron Lanthanide Phosphonate Clusters: $\{Fe_6Ln_6P_6\}$ Wells—Dawson-like Structures with D_{3d} Symmetry

Eufemio Moreno Pineda,[†] Floriana Tuna,[†] Yan-Zhen Zheng,[†,⊥] Simon J. Teat,[‡] Richard E. P. Winpenny,*[,†] Jürgen Schnack,[§] and Eric J. L. McInnes*[,†]

[†]School of Chemistry and Photon Science Institute, The University of Manchester, Oxford Road, Manchester M13 9PL, U.K.

[‡]Advanced Light Source, Lawrence Berkeley Laboratory, 1 Cyclotron Road, MS2-400, Berkeley, California 94720, United States

[§]Faculty of Physics, University of Bielefeld, Universitätsstr. 25, D-33615 Bielefeld, Germany

Supporting Information

ABSTRACT: Reaction of $[Fe_3(\mu_3\text{-}O)(O_2C^tBu)_6(HO_2C^tBu)_3](O_2C^tBu)$ and $[Ln_2(O_2C^tBu)_6(HO_2C^tBu)_6]$ (Ln = lanthanide) with three different phosphonic acids produce a family of highly symmetrical $\{Fe_6Ln_6P_6\}$ clusters with general formula $[Fe_6Ln_6(\mu_3\text{-}O)_2(CO_3)(O_3PR)_6(O_2C^tBu)_{18}]$, where R = methyl **1**, phenyl **2**, or *n*-hexyl **3**. All the clusters present an analogous metal frame to the previously reported $\{Ni_6Ln_6P_6\}$ both being related to the well-known Wells−Dawson ion from polyoxometallate chemistry. These highly symmetrical clusters have, or approximate very closely to, D_{3d} point symmetry. Both Fe^{III} and Gd^{III} ions are magnetically isotropic and could thus exhibit promising magnetocaloric properties; hence we investigated the $\{Fe_6Gd_6P_6\}$ compounds accordingly. Modeling the magnetic data of $[Fe_6Gd_6(\mu_3\text{-}O)_2(CO_3)(O_3PPh)_6(O_2C^tBu)_{18}]$ by the finite-temperature Lanczos method gave a strong antiferromagnetic Fe···Fe interaction ($J_{Fe-Fe} = -30$ cm^{-1}) and very weak Gd···Gd and Gd···Fe exchange interactions ($|J| < 0.1$ cm^{-1}). The strong antiferromagnetic Fe···Fe interaction could account for the relatively smaller $-\Delta S_m$ value observed, compared against the $\{Ni_6Gd_6P_6\}$ analogues.

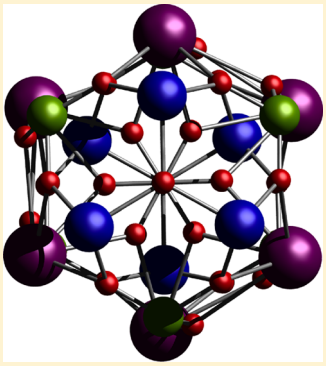

INTRODUCTION

The magnetic properties of molecular transition-metal cages have received a great deal of attention since it was demonstrated that some examples display memory effects, the so-called single molecule magnets.[1] This Study has led to research in related areas such as molecular spintronics, quantum information processing, and magnetocalorics.[1,2] We, and others, have been exploring the synthetic chemistry of 3d−4f cages to probe the effect of combining the very different magnetic properties of 3d and 4f ions in one molecule.[3,4] We have found that phosphonates, although usually requiring coligands to prevent formation of insoluble polymers, are particularly good ligands for binding such materials because the RPO_3^{2-} can bridge many metal ions, compared to carboxylates for example, with a favorable ligand set for the oxophilic lanthanides.[5,6] Moreover, their solubility and bulk can be readily tuned via choice of R, and it is also possible to introduce further functional groups.[6]

We recently reported a family of $\{Ni_6Gd_6P_6\}$ cages of general formula $[Ni^{II}_6Gd^{III}_6(\mu_3{-}OH)_2(O_3PR)_6(O_2C^tBu)_{16}(HO_2Ac)_2]$.[7] These molecules are both structurally and magnetically intriguing. Structurally, the molecules are layered, and if the phosphorus atoms are considered as part of the core then the 3:6:6:3 (Ni_3:Gd_3P_3:Gd_3P_3:Ni_3) structure strongly resembles that of the classic Wells−Dawson[8] $[X_2M_{18}O_{62}]^{n-}$ ion (X = e.g. P, Si), which may suggest wider correlation between phosphonate cages and polyoxometallate chemistry. Magnetically, the $\{Ni_6Gd_6P_6\}$ cages display rather large magnetocaloric effects (MCEs). The MCEs can be exploited in adiabatic demagnetisation experiments, and certain molecular cages have proved good candidates for very low-temperature refrigeration,[9] even at the molecular level,[10] due a highly degenerate set of low-lying spin states that can saturate in applied field, resulting in large magnetic entropy changes on application of an external magnetic field. In the case of $\{Ni_6Gd_6P_6\}$ the large MCE effects are due to a combination of the high spin multiplicity (Ni^{II}, S = 1; Gd^{III}, S = 7/2) and the presence of ferromagnetic internal coupling within the cage, meaning that relatively large magnetic entropy changes can be achieved with small applied field changes.

We have examined whether this Wells−Dawson-like family could be extended to other 3d metal systems. In this Work we report the successful replacement of the divalent Ni^{II} ions in $\{Ni_6Gd_6P_6\}$ for the isotropic trivalent Fe^{III}. This was to investigate (i) whether trivalent 3d ions could be incorporated into the same structure and, if so, how the differing charge balance would be accommodated and (ii) the effect on the magnetic, including magnetocaloric, behavior of replacing the anisotropic Ni^{II}, S = 1 spins with relatively isotropic and higher spin Fe^{III}, S = 5/2 spins. We further report substitution of the Gd^{III} ion with other 4f ions.

Received: November 13, 2013
Published: March 6, 2014

   dx.doi.org/10.1021/ic402839q | *Inorg. Chem.* 2014, 53, 3032−3038

Table 1. Crystallographic Information for Clusters 1−3 and 6

	1	2	3	6
chem formula	$Fe_6Gd_6P_6O_{60}C_{96}H_{180}$	$Fe_6Gd_6P_6O_{59}C_{127}H_{192}$	$Fe_6Gd_6P_6O_{59}C_{127}H_{240}$	$Fe_6Tb_6P_6O_{59}C_{127}H_{192}$
fw	3758.81	4127.21	4175.60	4137.23
cryst system	monoclinic	trigonal	trigonal	trigonal
space group	$P2_1/c$	$R\bar{3}c$	$R\bar{3}c$	$R\bar{3}c$
a/Å	15.590(3)	16.8883(3)	34.2470(4)	16.8951(2)
b/Å	15.565(3)	16.8883(3)	34.2470(4)	16.8951(2)
c/Å	31.774(6)	103.9530(2)	103.4064(12)	103.8149(15)
α/deg	90	90	90	90
β/deg	109.13(3)	90	90	90
γ/deg	90	120	120	120
V/Å^3	7285(3)	25676.6(11)	104667(3)	25663.2(7)
Z	2	6	24	6
ρ calcd/g cm^{-3}	1.714	1.601	1.590	1.606
T/K	173.0	100.0	100.0	100.0
μ (Mo Kα)/mm^{-1}	3.414	2.914	2.643	3.070
R_1 ($I > 2\sigma(I)$)[a]	0.0935	0.0717	0.0994	0.0950
wR_2[a]	0.2733	0.1433	0.2940	0.1972

[a] $R_1 = ||F_o| - |F_c||/|F_o|$, $wR_2 = [w(|F_o| - |F_c|)^2/w|F_o|^2]^{1/2}$

EXPERIMENTAL SECTION

Starting Materials. $[Fe^{III}_3(\mu_3\text{-}O)(O_2C^tBu)_6(HO_2C^tBu)_3](O_2C^tBu)$[11] and $[Ln^{III}_2(O_2C^tBu)_6(HO_2C^tBu)_6]$[12] (Ln = Gd, Tb, Dy, or Ho) were prepared by reported methods. All other starting materials and solvents were of reagent grade and used as purchased.

Synthetic Method. $[Fe^{III}_3(\mu_3\text{-}O)(O_2C^tBu)_6(HO_2C^tBu)_3](O_2C^tBu)$ (0.1 g, 0.075 mmol), $[Gd^{III}_2(O_2C^tBu)_6(HO_2C^tBu)_6]$ (0.1 g, 0.1 mmol), RPO_3H_2 (R = methyl, phenyl, or *n*-hexyl) (0.1 mmol), and triethylamine (0.1 mL, 1 mmol) in acetonitrile (8 mL) were stirred at room temperature for 5 min. The resulting slurry was transferred into a 10 mL Teflon-lined autoclave, which was heated at 150 °C for 12 h under solvothermal conditions[13] and then cooled to room temperature at a rate of 0.05 °C min^{-1}. Reddish-brown crystals (of X-ray diffraction quality) of $[Fe^{III}_6Gd^{III}_6(\mu_3\text{-}O)_2(O_2C^tBu)_{18}(O_3PR)_6(CO_3)]$, with R = Me (**1**), Ph (**2**), and *n*-hexyl (**3**) were obtained directly from the autoclave in 40−50% yield. Similar reactions with $[Ln^{III}_2(O_2C^tBu)_6(HO_2C^tBu)_6]$, where Ln = Tb, Dy, Ho, gave analogous $[Fe^{III}_6Ln^{III}_6(\mu_3\text{-}O)_2(O_2C^tBu)_{18}(O_3PR)_6(CO_3)]$ clusters (R = Me [Ln = Dy (**4**), Ho (**5**)] and Ph [Ln = Tb (**6**)]), in similar yields. (Elemental analyses and yields are in Supporting Information, Table S1; IR data are in Supporting Information, Figure S1.)

X-ray Data Collection and Structure Solution. Data for **1** were collected on a Bruker APEX II diffractometer (synchrotron, λ = 0.77490) at the Advanced Light Source, Berkeley Lab, U.S.A. Data reduction was performed with Bruker SAINT software. Single-crystal X-ray diffraction measurements for **2** and **6** were carried out on a Bruker SMART CCD diffractometer with Mo Kα radiation (λ = 0.71073 Å) at 100 K. Data for **3** were collected on a Rigaku Saturn724+ diffractometer (synchrotron, λ = 0.68890 Å) at beamline I19 at Diamond Light Source, U.K. Data reduction and unit cell refinement for **2**, **3**, and **6** were performed with Crysallis software. The structures were solved by direct methods using SHELXS-97[14a] and were refined by full-matrix least-squares methods using Olex2.[14b] In all cases the crystals were mounted on a tip using crystallographic oil and placed in a cryostream. Data were collected using ϕ and ω scans chosen to give a complete asymmetric unit. All non-hydrogen atoms were refined anisotropically. Hydrogen atoms were calculated geometrically and were riding on their respective atoms.

Some degree of disorder was found in all clusters. For compounds **2** and **6** the carbon atoms of the ^{t}Bu groups of the pivalate ligands are found to be disordered over two sites. The ^{t}Bu groups were modeled splitting their occupancy into parts. Bond and angle (DANG) and thermal (ISOR) restraints were also used to model these atoms. Some disorder was found on the oxygen atoms of the pivalates, which were also modeled splitting them into parts.

Reduction of the data of compound **1** yielded the nonstandard space group $P2_1/n$. Transformation of the unit cell from $P2_1/n$ to the standard space group $P2_1/c$ was performed with the matrix $\begin{pmatrix} 1 & 0 & 0 \\ 0 & 1 & 0 \\ 1 & 0 & 1 \end{pmatrix}$ using XPREP for posterior solution. Compound **1** was highly disordered, and some gadolinium and oxygen atoms were also modeled splitting their occupancy into parts. ISOR and DANG restraints were used to model some thermal ellipsoids. In this cluster we were not able to completely solve the carbonate group within the $\{Fe_6Gd_6P_6\}$ cage, probably due to the high level of disorder observed. Because of the hexyl chain on the R group in compound **3** more disorder was observed. ^{t}Bu and hexyl groups were restrained using (DANG), (ISOR), and (SADI) commands. The hexyl groups were also modeled using these commands. Several attempts to collect and solve diffraction data for clusters **4** and **5** were performed (see Supporting Information); however, due to the poor quality of the data we were not able to obtain the crystal structures. The unit cells of these compounds were obtained (see Supporting Information), having similar parameters to **1** confirming, along with the elemental analyses, that these are isostructural. Full crystallographic details can be found in CIF format: see the Cambridge Crystallographic Data Centre database (971523−971526) for **1**−**3** and **6**. Crystal data and refinement parameters are given in Table 1.

Magnetic Measurements. The magnetic properties of polycrystalline samples of **1**−**6** were measured with a Quantum Design MPMS-XL7 SQUID magnetometer. The samples were ground, placed in a gel capsule, and fixed with a small amount of eicosane to avoid movement during the measurement. The data were corrected for the diamagnetism from the gel capsule and the eicosane, with the diamagnetic contribution from the complexes calculated from Pascal constants.

RESULTS AND DISCUSSION

Synthetic Description. The $\{Ni_6Gd_6P_6\}$ family of clusters was prepared by reaction of a nickel carboxylate dimer, $[Ni^{II}_2(\mu_2\text{−}OH_2)(O_2C^tBu)_4(HO_2C^tBu)_4]$, with the gadolinium carboxylate dimer $[Gd^{III}_2(O_2C^tBu)_6(HO_2C^tBu)_6]$ and phosphonic acid with base in MeCN under solvothermal conditions.[7] To prepare analogous structures with trivalent d-block ions we replaced the nickel starting material with the most straightforward Fe^{III} carboxylates—the oxo-centered

dx.doi.org/10.1021/ic402839q | Inorg. Chem. 2014, 53, 3032−3038

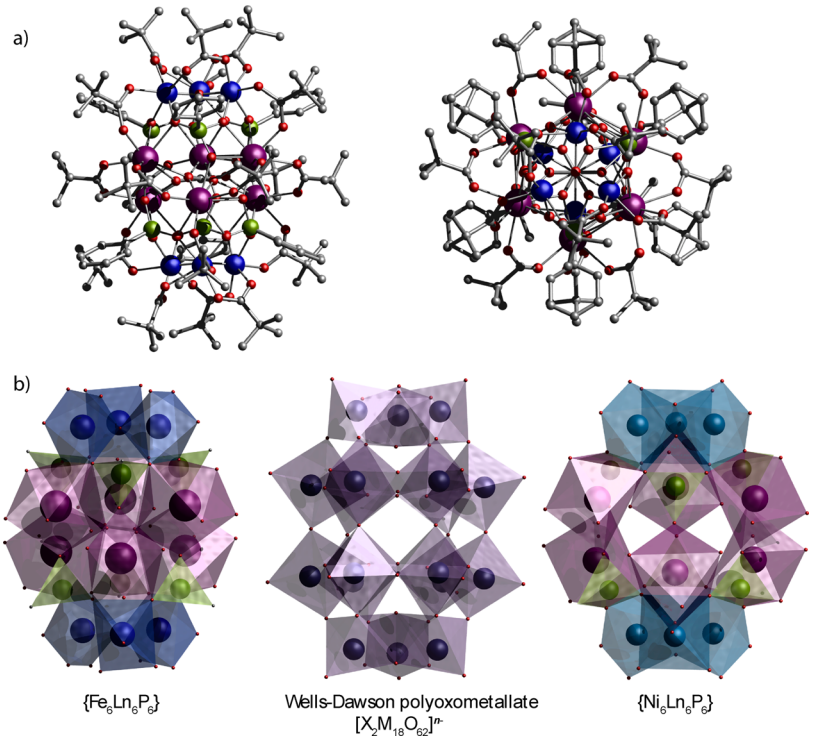

Figure 1. Crystal structure of the $\{Fe_6Gd_6P_6\}$ cage **2** viewed (a) (left) perpendicular to the C_3 axis and (right) down the C_3 axis. (b) Polyhedral representation of (left to right) $\{Fe_6Gd_6P_6\}$ core, Wells–Dawson polyoxometallate, and $\{Ni_6Gd_6P_6\}$ core. Colors: Gd, purple; Fe, blue; Ni, cyan; P, green; O, red; C, gray; H omitted for clarity.

triangles. Analogous solvothermal reactions with $[Fe^{III}_3(\mu_3\text{-}O)(O_2C^tBu)_6(HO_2C^tBu)_3](O_2C^tBu)$ successfully gave the $\{Fe_6Gd_6P_6\}$ clusters **1**–**3** in good yield (40–50%) in crystalline form directly on slowly cooling. Single-crystal X-ray diffraction identified the products as $[Fe^{III}_6Gd^{III}_6(\mu_3\text{-}O)_2(CO_3)(O_2C^tBu)_{18}(O_3PR)_6]$; these structures are much more symmetrical than their $\{Ni_6Gd_6P_6\}$ analogous (see Figure 1), and the key differences in the structures are detailed below. Attempts to extend the syntheses to other lanthanide ions (**4**–**6**) were only partially successful in terms of getting clean crystalline products; the reason for this is not clear.

Crystallography. Compounds **1**–**6** have very similar structures, and here we describe the structure of **2** in detail as representative (Figure 1 and Supporting Information, Figure S2). Compound **2** crystallizes in the $R\bar{3}c$ space group, and the molecule has crystallographic D_{3d} symmetry with only one Fe, one Gd, and one P in the asymmetric unit. (Compound **3** also crystallizes in the $R\bar{3}c$ space group, while **1** crystallizes in $P2_1/c$: although the latter then strictly has only C_{2h} point symmetry the structure is very close to D_{3d}). The cluster core then consists of 6 Fe^{III} and 6 Gd^{III} ions, bound by 6 phosphonates, 18 pivalates, and 2 oxides. The structure is layered, with two $\{Fe_3\}$ triangles capping two central Gd layers, overall giving a rugby ball-like shape (Figure 1). The $\{Fe_3\}$ and $\{Gd_3\}$ planes are separated by 3.677(3) Å, while the $\{Gd_3\}\cdots\{Gd_3\}$ interplane distance is 2.20(2) Å. The six Gd ions can alternatively be described as forming a ring in a chair conformation, with Gd···Gd edges of 3.931(2) Å. The two equilateral $\{Fe_3(\mu_3\text{-}O)\}$ triangles are oxo-centered with the $\mu_3\text{-}O^{2-}$ in the $\{Fe_3\}$ plane. The $\{Fe_3\}$ triangles sit eclipsed over the adjacent $\{Gd_3\}$ triangle (Figure 2 and Supporting Information, Figure S3) with nearest Fe···Gd distances of 3.677(3) Å. Each Fe···Fe edge (3.315(4) Å) is bridged by one pivalate (which adopts a 2.11 coordination mode in Harris notation)[15] and by two arms of a phosphonate. The phosphonates adopt a 5.222 coordination mode, further binding to two Gd^{III} ions in the adjacent $\{Gd_3\}$ layer and one in the other $\{Gd_3\}$ layer. The Gd and Fe ions are further bridged by 2.11 pivalates, as are the two $\{Gd_3\}$ layers. Finally, a carbonate ion is found in the middle of the cage, disordered over two sites, binding to all the Gd ions (6.222 binding mode). This must arise from atmospheric CO_2 fixation; there is ample precedent for this in lanthanide clusters.[16]

The $\{Gd_3\}$ and $\{P_3\}$ triangles in each half of the molecule are staggered with an interplane distance of just 1.485(1) Å. Hence, the alternating arrangement of Gd and P atoms can be defined as a puckered $\{Gd_3P_3\}$ ring. Treating the P atoms as part of the core in this way then gives a layered 3:6:6:3 $\{Fe_6Ln_6P_6\}$ structure which, as we noted for the $\{Ni_6Ln_6P_6\}$ family, strongly resembles the Wells–Dawson polyoxometallate (Figure 1b).

The additional 6+ charge on the $\{M_6Ln_6P_6\}$ core of $\{Fe_6Ln_6P_6\}$ cf. $\{Ni_6Ln_6P_6\}$ requires changes in the ligand set to retain charge balance (Figure 2): (i) The $\{Fe_3\}$ triangles in $\{Fe_6Ln_6P_6\}$ incorporate μ_3-oxide rather than μ_3-hydroxide as in the equivalent $\{Ni_3\}$ triangles, presumably carrying through from the $\{Fe_3O\}$ starting material. As a consequence, the $\{Fe_3O\}$ fragments are planar, while in $\{Ni_3(OH)\}$ the hydroxide is displaced ca. 0.5 Å from the $\{Ni_3\}$ plane toward the center of the cage (Figure 2a). (ii) In the $\{Ni_3\}$ triangles of $\{Ni_6Ln_6P_6\}$ two edges have conventional 1,3-carboxylate bridges (2.11 binding mode in Harris notation), but the third edge has instead a 1,1-bridging carboxylic acid (i.e., via a single O atom; 2.20 binding) (Figure 2c). This makes the $\{Ni_3\}$ triangle isosceles, with the unique edge ca. 0.3 Å shorter than the other two (Ni···Ni distances ca. 3.15 and 3.45 Å). In $\{Fe_6Ln_6P_6\}$ all the carboxylates are 1,3-bridges, and the $\{Fe_3\}$

dx.doi.org/10.1021/ic402839q | Inorg. Chem. 2014, 53, 3032–3038

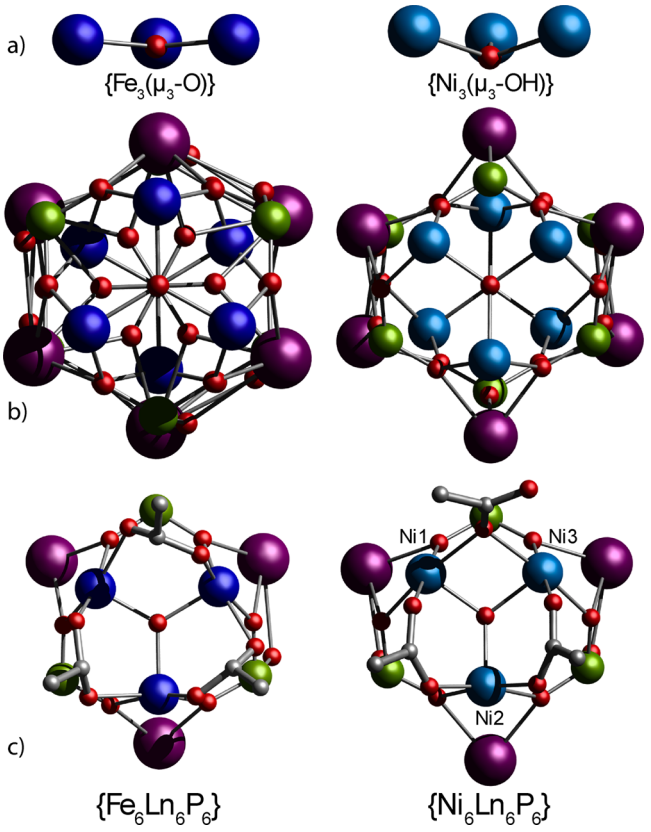

Figure 2. Comparison of $\{Fe_6Gd_6P_6\}$ and $\{Ni_6Gd_6P_6\}$. (a) $\{Fe_3(\mu_3\text{-}O)\}$ (left) and $\{Ni_3(\mu_3\text{-}O)\}$ (right) fragments; (b) $\{Fe_6Gd_6P_6\}$ viewed down the C_3 axis (left) and equivalent $\{Ni_6Gd_6P_6\}$ (right); (c) $\{Fe_3Gd_3P_3\}$ (left) and $\{Ni_3Gd_3P_3\}$ (right) fragments (the Ni1···Ni3 edge is unique with a 1,1-bridging carboxylic acid). Colors: Gd, purple; Fe, blue; Ni, cyan; P, green; O, red; C, gray; H omitted for clarity.

triangle is equilateral. (iii) The Ln sites in the $\{Ni_6Ln_6P_6\}$ cages are seven-coordinate, with a capped octahedral geometry, while in the $\{Fe_6Ln_6P_6\}$ the Ln sites are eight-coordinate with a dodecahedral coordination geometry.

These changes to the ligand set are accompanied by less variation in the phosphonate binding modes in $\{Fe_6Ln_6P_6\}$. In $\{Ni_6Ln_6P_6\}$ two binding modes are observed: each half of the molecule has two 5.222 phosphonates (as in $\{Fe_6Ln_6P_6\}$) while the third (on the unique Ni···Ni edge) is only 5.221 bound. In $\{Fe_6Ln_6P_6\}$ all the phosphonates are equivalent and 5.222 bound (Supporting Information, Figure S3). This affects the Ln···Ln distances; for example, in the $\{Fe_6Gd_6P_6\}$ complex **2** these are 3.931(2) Å, each pair being bridged by one 1,1 arm of a phosphonate (i.e., single-atom bridging) and one 1,3-bridging phosphonate (Supporting Information, Figure S3). In the $\{Ni_6Gd_6P_6\}$ complex with the same phosphonate (R = Ph) there are two Gd···Gd edges of 3.889(1) Å and four that are much longer (5.035(1) and 5.018(1) Å) corresponding to two 1,3-bridging phosphonates. Finally, the nearest neighbor Fe···Ln distances are slightly longer than Ni···Ln, for example, 3.677(3) Å in **2** and 3.360(2) to 3.509(2) Å in the equivalent $\{Ni_6Gd_6P_6\}$ molecule.

The net result of these changes is that $\{Fe_6Ln_6P_6\}$ is a much more regular and higher-symmetry system compared to $\{Ni_6Ln_6P_6\}$. Schematically, $\{Fe_6Ln_6P_6\}$ is an equilateral trigonal antiprism (D_{3d}; crystallographically imposed for **2** and **3**) while $\{Ni_6Ln_6P_6\}$ is an isosceles trigonal antiprism (C_{2h}, with the 2-fold axis corresponding to one of the perpendicular C_2' axes of the D_{3d} structure; crystallographically there is only inversion symmetry). This has direct consequences for the magnetic interactions in the molecules.

Magnetic Description. Magnetic susceptibility studies on **1**−**6** were performed on polycrystalline samples in the temperature range of 1.8−300 K under an applied direct-current (dc) magnetic field (H) of 1000 Oe. Magnetisation as a function of applied field was investigated in the field and in the temperature ranges of 0−7 T and 2−10 K, respectively (Figure 3 and Supporting Information, Figure S4).

For **1**−**3**, room-temperature $\chi_M T$ values (where χ_M is the molar magnetic susceptibility) of 52.4, 51.1, and 52.3 emu K mol^{-1}, respectively, were observed. These values are substantially lower than those calculated for the sum of six independent Fe^{III} (S = 5/2) and six Gd^{III} (S = 7/2) centers (73.5 emu K mol^{-1}, assuming g = 2.0 for both ions), but they are only slightly higher than expected for six Gd^{III} ions (47.25 emu K mol^{-1}). On cooling, the $\chi_M T$ products decrease relatively slowly until ca. 20 K, below which they decrease more rapidly, reaching 37.2, 27.8, and 36.5 emu K mol^{-1} for **1**−**3**, respectively, at 2 K. The molar magnetization (M) as a function of applied field at base temperature (2 K) rises slightly more slowly than the calculated Brillouin function for six noninteracting Gd^{III} (Figure 3), and the saturation values (at $\mu_0 H >$ ca. 4 T) are only slightly higher than they are for six Gd^{III} ions (42 μ_B), being 44.9, 43.4, and 44.9 μ_B for **1**−**3**, respectively.

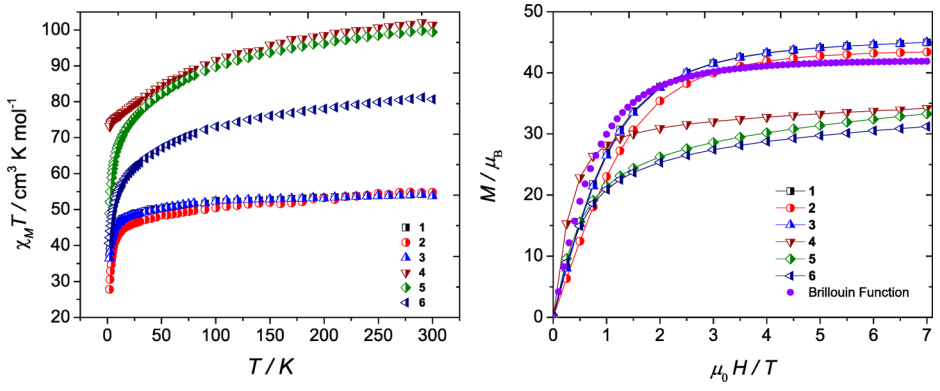

Figure 3. (left) Molar magnetic susceptibility ($\chi_M T$) vs T plot for **1**−**6** under 1 kG dc field. (right) Molar magnetization (M) as a function of applied magnetic field (H) at 2 K for **1**−**6**.

dx.doi.org/10.1021/ic402839q | Inorg. Chem. 2014, 53, 3032−3038

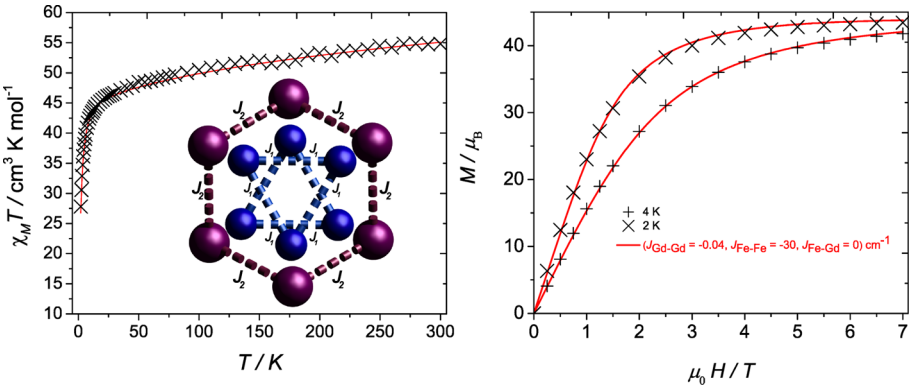

Figure 4. The (left) $\chi_M T(T)$ and (right) $M(H,T)$ fittings for compound **2**. (inset) Schematic sketch of the magnetic core **1**−**3**; dashed lines indicate exchange interactions. The J_3 coupling (not shown) acts between nearest Fe and Gd ions.

Hence, the $\chi_M T(T)$ and $M(H)$ behaviors are dominated by the six Gd^{III} ions. This implies that the magnetic moments due to the six Fe^{III} ions are largely canceled out by comparatively strong antiferromagnetic interactions. If we assume that each $\{Fe_3\}$ triangle is strongly coupled with an $S = 1/2$ ground state, the saturation magnetization at 2 K corresponds to the sum of six $S = 7/2$ and two $S = 1/2$ centers, which is 44 μ_B (for g = 2.0), close to the experimental values.

As a representative example, the magnetic behavior of **2** was modeled with an isotropic Heisenberg Hamiltonian:

$$\hat{H} = -2\sum_{i<j} J_{ij}\hat{S}_i \cdot \hat{S}_J + g\mu_B B S_z \quad (1)$$

Here $\hat{s}_i$ denotes the individual spin operators at site i (7/2 or 5/2) and $\hat{S}_z$ denotes the z component of the total spin operator. Because the dimension of the Hilbert space is a staggering 12 230 590 464, an exact matrix diagonalization is impossible, but observables can be approximated using the finite-temperature Lanczos method (FTLM).[17] We considered three possible distinct exchange interactions: J_1 within the $\{Fe_3\}$ triangles, J_2 between nearest Gd ions within the buckled $\{Gd_6\}$ ring, and J_3 between each Fe ion and the closest Gd ion on the $\{Gd_6\}$ ring (Figure 4 and Supporting Information, Figure S5). An isotropic g = 2.00 was used. The poor radial extent of the Gd 4f functions means that $|J_2|$ and $|J_3|$ are likely to be very small; hence, J_1 is the dominant interaction. If we assume $J_3 = 0$, to make the calculations relatively simple, then good simultaneous agreement with the experimental $\chi_M T(T)$ and $M(H)$ data is obtained with antiferromagnetic exchange interactions of $J_1 = -30$ cm^{-1} and $J_2 = -0.04$ cm^{-1} (Figure 4). If we instead assume $J_2 = 0$, then we get a poorer approximation both in $\chi_M T(T)$ and $M(H)$ (Supporting Information, Figure S5). We then investigated parameters sets allowing both J_2 and J_3 to be nonzero, with J_2 varied in a narrow range of about −0.04 cm^{-1} (Supporting Information, Figure S5). To summarize, good results could be obtained with nonzero $|J_3| < 0.1$ cm^{-1}, in accord with earlier findings in 3d−4f cages[3d] and with slightly better agreement for ferromagnetic coupling, with a slight decrease in the magnitude of J_2. A larger antiferromagnetic J_3 coupling can be excluded because then the magnetization rises too slowly with applied field. A similar reason precludes smaller Fe···Fe (J_1) couplings because then the magnetization would rise to much larger values.

The very weak J_1 and J_2 interactions involving Gd ions is expected. The Fe···Fe exchange is typical of that in the classic basic metal carboxylate triangles $[Fe_3(\mu_3\text{-}O)(O_2CR)_6L_3]^+$;[18] this is at first surprising because the exchange interaction mediated by phosphonates is generally much weaker than that by carboxylates. However, the triangular fragments in **1**−**3** can be written as $[Fe_3(\mu_3\text{-}O)(O_2C^tBu)_3(O_2P(O)R)_3(O_2C^tBu)_3]$ where the first three carboxylates are 1,3-bridging within the triangle, while the second set of carboxylates are the "terminal" ligands; that is, they do not bridge within the triangle. Hence, with respect to $[Fe_3(\mu_3\text{-}O)(O_2CR)_6L_3]^+$, we have simply replaced three 1,3-bridging carboxylates for 1,3-bridging phosphonates. Presumably the exchange interaction is carried predominantly by the oxide and remaining 1,3-bridging carboxylates.

To assess the magnetocaloric behavior of **1**−**3**, the magnetic entropy changes were determined indirectly from the magnetization as a function of applied field and temperature data using the Maxwell relationship $-\Delta S_m = \int[\partial M(T,M)/\partial T]_H \, dH$ (Supporting Information, Figure S4). We obtain maximum magnetic entropy changes for ΔH = 0−7 T at 3 K of $-\Delta S_m$ = 25.4, 22.0, and 22.9 J kg^{-1} K^{-1} for **1**−**3**, respectively. The larger value for **1** is simply because of its lower molecular weight (phosphonate substituent R = Me vs Ph, hexyl): in molar units we have 95.1, 90.8, and 95.6 J mol^{-1} K^{-1}, respectively.

It is instructive to compare these results to those for $\{Ni_6Gd_6P_6\}$ under the same experimental conditions: these are in the range of 105−116 J mol^{-1} K^{-1}, depending on R. Hence, we have much larger magnetic entropy changes for $\{Ni_6Gd_6P_6\}$ cf. $\{Fe_6Gd_6P_6\}$ despite the lower spin and greater magnetic anisotropy of Ni^{II} cf. Fe^{III}. Moreover, for the former we are accessing much more of theoretically possible magnetic entropy given by the total multiplicity of the spin system, $S_m = \Pi_i \ln(2S_i + 1)$ R (where R is the gas constant). For $\{Fe_6Gd_6P_6\}$ with six S = 5/2 and six S = 7/2 centers, this gives S_m = 193 J mol^{-1} K^{-1}. Hence, under our experimental magnetization conditions we are only accessing ca. 50% of the available magnetic entropy. For $\{Ni_6Gd_6P_6\}$ with six S = 1 and six S = 7/2 centers, this gives S_m = 159 J mol^{-1} K^{-1}. Hence, for these compounds we are accessing ca. 70% of the available magnetic entropy.

This can be explained by the strength of the exchange interaction within the 3d metal $\{M_3\}$ triangles. For $\{Fe_6Gd_6P_6\}$ we have $J_{Fe-Fe} = -30$ cm^{-1} (see above). For an isolated equilateral $\{Fe_3\}$ triangle this would give a doubly degenerate total spin S = 1/2 ground state, with the lowest excited states (S = 3/2) at 90 cm^{-1}. At low temperature only the S = 1/2 states are accessible, even at high field. Magnetic data for $\{Ni_6Gd_6P_6\}$ could only be modeled with two unique J_{Ni-Ni} exchange values, consistent with the isosceles $\{Ni_3\}$ symmetry: two interactions

dx.doi.org/10.1021/ic402839q | Inorg. Chem. 2014, 53, 3032−3038

of +2 to +5 cm^{-1} (depending on R), and one interaction of −1 to −4 cm^{-1} (depending on R). For an isolated $\{Ni_3\}$ triangle this would give the entire 27-fold energy spectrum within 30−60 cm^{-1} (depending on R). There are two important points: (i) the couplings are much weaker for Ni, and (ii) there are ferromagnetic interactions for Ni. These result in a much greater proportion of the magnetic spectrum (and hence the proportion of the possible magnetic entropy) being accessible at low temperature and low field, combined with the ability to fully saturate the magnetization (M = 55 μ_B at 7 T and 2 K for $\{Ni_6Gd_6P_6\}$, consistent with the full alignment of spins). These two factors enhance the magnetocaloric response for $\{Ni_6Gd_6P_6\}$ cf. $\{Fe_6Gd_6P_6\}$, far outweighing the effect of the lower spin of Ni^{II}. These factors also override the significant zero-field splittings of Ni^{II}, which are in the range of 4−6 cm^{-1}, from magnetic studies of $\{Ni_6Y_6P_6\}$. The Fe^{III} ions in $\{Fe_6Gd_6P_6\}$ could be treated as isotropic.

Comparing the molar magnetic entropy for compounds **1**−**3**, it is clear than the value obtained for **2** is lower than that for **1** and **3**. This has also been observed in $\{Ni_6Gd_6P_6\}$ where the magnetic entropy of the phenyl phosphonate cluster was slightly lower than that of the alky-phosphonate analogues. Comparing the magnetic data for **1**−**3** we can see that $\chi_M T(T)$ and $M(H)$ are lower for **2** than they are for **1** and **3**, suggesting slightly stronger antiferromagnetic interactions within the cluster.

The $\chi_M T$ values at room temperature for **4**−**6** were: for **4**, 101.4 emu K mol^{-1} (calcd. 111.25 emu K mol^{-1} for six Fe^{III}, g = 2.00, S = 5/2 and six Dy^{III}, g_J = 4/3, J = 15/2); for **5**, 99.4 emu K mol^{-1} (calcd. 110.6 emu K mol^{-1} for six Fe^{III}, g = 2.00, S = 5/2 and six Ho^{III}, g_J = 5/4, J = 8); and for **6**, 80.7 emu K mol^{-1} (calcd. 97.1 emu K mol^{-1} for six Fe^{III}, g = 2.00, S = 5/2 and six Tb^{III}, g_J = 3/2, J = 6). All these experimental room-temperature values are lower than the sum of the constituent ions, again likely due to the magnitude of the antiferromagnetic exchange interaction within the $\{Fe_3O\}$ moieties. In magnetization experiments $M(H)$ for **4**−**6** at 2 K reaches values of 34.2, 33.3, and 31.2 μ_B, respectively, at 7 T. None of the clusters showed any out-of-phase response in alternating-current susceptibility measurements down to 2 K.

CONCLUSIONS

Substitution of the nickel dimer starting material for an iron source allowed us to synthesize a family of $\{Fe_6Ln_6P_6\}$ cages with a metal core analogous to the $\{Ni_6Ln_6P_6\}$ and the well-known Wells−Dawson polyoxometallates. These clusters are more symmetrical than the nickel counterparts, possessing D_{3d} point symmetry. Structurally three differences distinguish the $\{Fe_6Ln_6P_6\}$ from the $\{Ni_6Ln_6P_6\}$ clusters: the presence of 18 carboxylates, 2 oxides, and 1 carbonate charge balancing the cage. Simultaneous fitting of the magnetic data $\chi_M T(T)$ and $M(H)$ showed strong antiferromagnetic interactions between the Fe···Fe pairs ($J_{Fe\cdots Fe}$ = −30 cm^{-1}), which are responsible for the lower observed MCE response than in $\{Ni_6Gd_6P_6\}$ despite introducing a more isotropic ion with higher spin multiplicity (Fe^{III}, S = 5/2, $^6S_{5/2}$). The model assumes an equilateral $\{Fe_3\}$ triangle, consistent with the crystallography, which would be a highly frustrated system with a doubly degenerate pair of S = 1/2 states at lowest energy;[19] Type 1 frustration by the classification we have recently introduced.[20] In general $\{Fe_3\}$ triangles show distortions at low temperature,[18] losing the degeneracy. The results we report here do not suggest any such distortion; however, we have not yet been able to make the Wells−Dawson structure for $\{Fe_6Y_6P_6\}$, which would allow us to investigate the frustration more carefully, for example by electron paramagnetic resonance spectroscopy.

ASSOCIATED CONTENT

Supporting Information

This includes cif files, further synthetic details, structural drawings, further modeling of magnetic data, and magnetic plots. This material is available free of charge via the Internet at http://pubs.acs.org.

AUTHOR INFORMATION

Corresponding Authors

*E-mail: eric.mcinnes@manchester.ac.uk (E.J.L.M.).
*E-mail: richard.winpenny@manchester.ac.uk (R.E.P.W.).

Present Address

⊥Center for Applied Chemical Research, Frontier Institute of Science and Technology, Xi'an Jiaotong University, Xi'an 710054, China.

Notes

The authors declare no competing financial interest.

ACKNOWLEDGMENTS

E.M.P. thanks the Panamanian agency SENACYT-IFARHU. J.S. thanks the Deutsche Forschungsgemeinschaft (SCHN/615-15) for continuous support. Supercomputing time at the LRZ Garching (Germany) is gratefully acknowledged. R.E.P.W. thanks the Royal Society for a Wolfson Merit Award. We also thank Dr. David Allan and his team for help in use of X-ray at the synchrotron at Diamond Light Source, and we thank DLS for beam-time. The ALS is supported by the Director, Office of Science, Office of Basic Energy Sciences, of the U.S. Department of Energy under Contract No. DE-AC02-05CH11231.

REFERENCES

(1) Gatteschi, D.; Sessoli, R.; Villain, J. *Molecular Nanomagnets;* Oxford University Press: Oxford, 2006.

(2) Winpenny, R. E. P.; McInnes, E. J. L. Molecular Nanomagnets. In *Molecular Materials;* Walton, R.I.; Bruce, D.W.; O'Hare, D., Eds.; Inorganic Materials Series; Wiley: New York, 2010, Vol. 3.

(3) (a) Zhang, Z.-M.; Pan, L.-Y.; Lin, W.-Q.; Leng, J.-D.; Guo, F.-S.; Chen, Y.-C.; Liu, J.-L.; Tong, M.-L. *Chem. Commun.* **2013**, *49*, 8081. (b) Karotsis, G.; Evangelisti, M.; Dalgarno, S. J.; Brechin, E. K. *Angew. Chem., Int. Ed.* **2009**, *48*, 9928. (c) Langley, S. K.; Chilton, N. F.; Moubaraki, B.; Hooper, T.; Brechin, E. K.; Evangelisti, M.; Murray, K. S. *Chem. Sci.* **2011**, *50*, 6606. (d) Hooper, T. N.; Schnack, J.; Pilgkos, S.; Evangelisti, M.; Brechin, E. K. *Angew. Chem., Int. Ed.* **2012**, *51*, 4633. (e) Peng, J.-P.; Zhang, Q.-C.; Kong, X.-J.; Zheng, Y.-Z.; Ren, Y.-P.; Long, L.-S.; Huang, R.-B.; Zheng, L.-S.; Zheng, Z. *J. Am. Chem. Soc.* **2012**, *134*, 3314. (f) Peng, J.-B.; Zhang, Q.-C.; Kong, X.-J.; Ren, Y.-P.; Long, L.-S.; Huang, R.-B.; Zheng, L.-S.; Zheng, Z. *Angew. Chem., Int. Ed.* **2011**, *50*, 10649. (g) Zheng, Y.; Zhang, Q.-C.; Long, L.-S.; Huang, R.-B.; Müller, A.; Schnack, J.; Zheng, L.-S.; Zheng, Z. *Chem. Commun.* **2013**, *49*, 36.

(4) For example: (a) Mondal, K. C.; Sund, A.; Lan, Y.; Kostakis, G. E.; Waldmann, O.; Ungur, L.; Chibotaru, L. F.; Anson, C. E.; Powell, A. K. *Angew. Chem., Int. Ed.* **2012**, *51*, 7550. (b) Costes, J.-P.; Vendiera, L.; Wernsdorfer, W. *Dalton Trans.* **2011**, *40*, 1700. (c) Mondal, K. C.; Kostakis, G. E.; Lan, Y.; Wernsdorfer, W.; Anson, C. E.; Powell, A. K. *Inorg. Chem.* **2011**, *50*, 11604.

(5) For example: (a) Baskar, V.; Gopal, K.; Helliwell, M.; Tuna, F.; Wernsdorfer, W.; Winpenny, R. E. P. *Dalton Trans.* **2010**, *39*, 4747. (b) Wang, M.; Yuan, D.-Q.; Ma, C.-B.; Yuan, M.-J.; Hu, M.-Q.; Li, N.; Chen, H.; Chen, C.-N.; Liua, Q.-T. *Dalton Trans.* **2010**, *39*, 7276.

(c) Zheng, Y.-Z.; Evangelisti, M.; Winpenny, R. E. P. *Chem. Sci.* **2011**, *2*, 99. (d) Zheng, Y.-Z.; Pineda, E. M.; Helliwell, M.; Evangelisti, M.; Winpenny, R. E. P. *Chem.—Eur. J.* **2012**, *18*, 4161. (e) Zheng, Y.-Z.; Evangelisti, M.; Tuna, F.; Winpenny, R. E. P. *J. Am. Chem. Soc.* **2012**, *134*, 1057.

(6) Pineda, E. M.; Tuna, F.; Pritchard, R. G.; Regan, A. C.; Winpenny, R. E. P.; McInnes, E. J. L. *Chem. Commun.* **2013**, *49*, 3522.

(7) (a) Zheng, Y.-Z.; Evangelisti, M.; Winpenny, R. E. P. *Angew. Chem., Int. Ed.* **2011**, *50*, 3692. (b) Pineda, E. M.; Tuna, F.; Zheng, Y.-Z.; Winpenny, R. E. P.; McInnes, E. J. L. *Inorg. Chem.* **2013**, *52*, 13702.

(8) An anion with a formula of $X_2M_{18}O_{62}^{n-}$, where X = P, Si, and As, M = Mo and W, see Pope, M. T. *Heteropoly and Isopoly Oxometalate;* Springer: New York, 1983.

(9) (a) Sharples, J. W.; Collison, D. *Polyhedron* **2013**, *54*, 91. (b) Sessoli, R. *Angew. Chem., Int. Ed.* **2012**, *51*, 43. (c) Evangelisti, M.; Brechin, E. K. *Dalton Trans.* **2010**, *39*, 4672. (d) Evangelisti, M.; Candini, A.; Ghirri, A.; Affronte, M.; Brechin, E. K.; McInnes, E. J. L. *Appl. Phys. Lett.* **2005**, *87*, 072504. (e) Garlatti, E.; Carretta, S.; Schnack, J.; Amoretti, G.; Santini, P. *Appl. Phys. Lett.* **2013**, *103*, 202410.

(10) Corradini, V.; Ghirri, A.; Candini, A.; Biagi, R.; del Pennino, U.; Dotti, G.; Otero, E.; Choueikani, F.; Blagg, R. J.; McInnes, E. J. L.; Affronte, M. *Adv. Mater.* **2013**, *25*, 2816.

(11) (a) Gerbeleu, N. V.; Batsanov, A. S.; Timko, G. A.; Struchkov, Y. T.; Indrichan, K. M.; Popovich, G. A. *Dokl. Akad. Nauk SSSR* **1987**, *293*, 364. (b) Tolis, E. I.; Helliwell, M.; Langley, S.; Raftery, J.; Winpenny, R. E. P. *Angew. Chem., Int. Ed.* **2003**, *42*, 3804.

(12) (a) Fomina, I. G.; Kiskin, M. A.; Martynov, A. G.; Aleksandrov, G. G.; Dobrokhotova, Z. V.; Gorbunova, Y. G.; Shvedenkov, Y. G.; Tsivadze, A. Y.; Novotortsev, V. M.; Eremenko, I. L. *Zh. Neorg. Khim.* **2004**, *49*, 1463. (b) Zoan, T. A.; Kuzmina, N. P.; Frolovskaya, S. N.; Rykov, A. N.; Mitrofanova, N. D.; Troyanov, S. I.; Pisarevsky, A. P.; Martynenko, L. I.; Korenev, Y. M. *J. Alloys Compd.* **1995**, *225*, 396.

(13) Laye, R. H.; McInnes, E. J. L. *Eur. J. Inorg. Chem.* **2004**, *14*, 2811.

(14) (a) Sheldrick, G. M. *Acta Crystallogr.* **2008**, *A64*, 112. (b) Dolomanov, O. V.; Bourthis, L. J.; Gildea, R. L.; Howard, J. A. K.; Puschmann, H. *J. Appl. Crystallogr.* **2009**, *42*, 339.

(15) $X.Y_1Y_2Y_3$ where X is the total number of metal ions bound by the ligand, and Y values refer to the number of metal ions attached to the different donor atoms: Coxall, R. A.; Harris, S. G.; Henderson, D. K.; Parsons, S.; Tasker, P. A.; Winpenny, R. E. P. *J. Chem. Soc., Dalton Trans.* **2000**, 2349.

(16) For example: (a) Langley, S. K.; Moubaraki, B.; Murray, K. S. *Inorg. Chem.* **2012**, *51*, 3947. (b) Sakamoto, S.; Fujinami, T.; Nishi, K.; Matsumoto, N.; Mochida, N.; Ishida, T.; Sunatsuki, Y.; Re, N. *Inorg. Chem.* **2013**, *52*, 7218. (c) Bag, P.; Dutta, S.; Biswas, P.; Maji, S. K.; Flörkec, U.; Nag, K. *Dalton Trans.* **2012**, *41*, 3414. (d) Barrett-Adams, D. M. Y.; Kahwa, I. A.; Mague, J. T. *New J. Chem.* **1998**, 919.

(17) (a) Jaklič, J.; Prelovšek, P. *Phys. Rev. B: Condens. Matter Mater. Phys.* **1994**, *49*, 5065. (b) Schnack, J.; Wendland, O. *Eur. Phys. J. B* **2010**, *78*, 535−541.

(18) Cannon, R. D.; White, R. P. *Prog. Inorg. Chem.* **1988**, *36*, 195.

(19) (a) Mentrup, D.; Schmidt, H.-J.; Schnack, J.; Luban, M. *Phys. A* **2000**, *278*, 214. (b) Bärwinkel, K.; Hage, P.; Schmidt, H.-J.; Schnack, J. *Phys. Rev. B: Condens. Matter Mater. Phys.* **2003**, *68*, 054422.

(20) Baker, M. L.; Timco, G. A.; Piligkos, S.; Mathieson, J.; Mutka, H.; Tuna, F.; Kozłowski, P.; Antkowiak, M.; Guidi, T.; Gupta, T.; Rath, H.; Woolfson, R. J.; Kamieniarz, G.; Pritchard, R. G.; Weihe, H.; Cronin, L.; Rajaraman, G.; Collison, D.; McInnes, E. J. L.; Winpenny, R. E. P. *Proc. Natl. Acad. Sci.* **2012**, *109*, 19113.